ACS OMEGA

Open Access

http://pubs.acs.org/journal/acsodf

Article

Optimizing the Shell Thickness of Ag@TiO_2 Nanostructures by a Simple Top-Down Method to Engineer Effective SERS Substrates and Photocatalysts

Mahabubur Rahman, Md Al-Amin, Amandeep Kaur, Shirin Akter Jahan, Andrew J. Wilson, and Nur Uddin Ahamad*

Cite This: *ACS Omega* 2025, 10, 14940−14948

Read Online

ACCESS | Metrics & More | Article Recommendations | Supporting Information

ABSTRACT: In this article, we discuss a simple method to prepare core−shell Ag@TiO_2 nanoparticles (NPs) with an optimized shell thickness to engineer plasmonic photocatalysts and surface-enhanced Raman scattering (SERS) substrates. Variation in the shell (TiO_2) thickness was analyzed by an acid-etching method, and the deterioration of the shell was traced by monitoring the extinction spectra of both colloidal and solid-supported Ag@TiO_2 NPs. Attainment of the optimum shell thickness was confirmed by noticing the simultaneous appearance of the LSPR absorption band (at 450 nm) of core silver nanostructures (d = ∼10 nm) and the scattering signature of the shell (TiO_2) in the extinction spectrum of Ag@TiO_2 NPs. This study showed that the optimum thickness of TiO_2 is ∼2 nm, which allowed LSPR excitation by visible light. The observed blue shift of the LSPR peak, compared to the unetched Ag@TiO_2 NPs, with etching time indicated the size reduction of the NPs. Ag@TiO_2 with the optimum thickness exhibited a reaction rate five times faster than that of unetched Ag@TiO_2 under visible light irradiation. Ag@TiO_2 NPs exhibited higher photocatalytic activity under visible light irradiation than under UV light. Furthermore, Ag@TiO_2 NPs with the optimized thickness exhibited significantly higher SERS activity than the unetched Ag@TiO_2 NPs. The elevated photocatalytic and SERS activities exhibited by engineered Ag@TiO_2 NPs reveal the effectiveness of the etching process in creating a plasmonic effect in core(plasmonic)−shell (semiconductor) nanostructures.

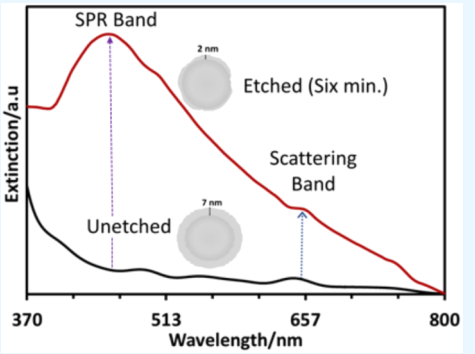

1. INTRODUCTION

Light trapping and subsequent local electromagnetic (EM) field enhancement capabilities of noble metal nanostructures (Ag, Au, Cu, etc.) have made them a unique class of materials termed plasmonic materials.[1] Interaction of light with metal nanoparticles results in surface plasmon excitation that is confined at the metal−dielectric interface.[2] When the frequency of incident light matches the surface plasmon modes, light energy is absorbed by the nanoparticles, and an intense local electromagnetic field is generated. Such a phenomenon is called surface plasmon resonance (SPR). Under SPR conditions, an absorption band or peak appears in the absorption spectrum of plasmonic materials.[3] The interesting property that makes the plasmonic materials so precious is that the position and number of surface plasmon absorption peaks depend on the material, size, shape, and the refractive index of an external medium.[3] Using this unique property of plasmonic nanostructures, several techniques have been developed, such as SERS and SPR sensors.[1,2] The electromagnetic field generated under the SPR conditions is distance-dependent i.e., the EM field is intense at the surface and diminishes away from it.[3] Another interesting phenomenon appears when a plasmonic nanostructure is brought into contact with a semiconductor metal oxide (MO); at the interface, a Schottky barrier (SB) is formed. When photoexcited plasmon decay occurs, hot electrons are generated in metal nanoparticles. These hot electrons can be collected by placing an appropriate semiconductor in contact with the metal.[4] These high-energy electrons can surmount the SB and be injected into the semiconductor, increasing its charge carriers (electron−hole). These electron−hole pairs can be utilized in developing photovoltaic and photocatalytic devices.[5,6] Core−shell nanostructures consisting of metal−metal oxides offer several advantages: the Schottky barrier at the interface that allows hot electron transfer upon excitation of surface plasmons by light, the plasmonic response of core metal can be tuned by optimizing the shell thickness and the inert shell composed of MO increases the stability of core

Received: November 12, 2024
Revised: March 22, 2025
Accepted: March 26, 2025
Published: April 13, 2025

https://doi.org/10.1021/acsomega.4c10276
ACS Omega 2025, 10, 14940−14948

metals by reducing the leakage of toxic metal ions and withstand the oxidation of metals.[6] Moreover, the oxide shell renders the possibility of surface functionalization with interested molecules, which finds applications in SERS and SPR-based molecular detection.[7−11] Core−shell nanoparticles consisting of Ag@TiO_2 provide additional benefits. Ag is a well-known plasmonic material with a wide range of SPR absorption abilities, and TiO_2 is a good electron-accepting MO because of its high density of states in the conduction band.[1,12] Hot electrons generated by silver nanoparticles have enough energy to overcome the SB formed at the interface of Ag and TiO_2, which facilitates injection of hot electrons into TiO_2.[13,14] Controlling the thickness of the shell can be achieved by several methods, such as layer-by-layer or bottom-up synthesis of core−shell nanoparticles with different thicknesses.[6,15,16] However, the top-down method is rare. Therefore, in this research, a simple but effective method is demonstrated to control the thickness of the shell in Ag@TiO_2 nanoparticles by an acid etching process. The desired shell (TiO_2) is achieved by monitoring the absorption spectrum of silver nanoparticles both in solution and on solid supports. The core−shell nanostructures with the optimized shell thickness provide a platform to architect improved SERS enhancement and photocatalysis.

2. MATERIALS AND METHODS

2.1. Chemicals. Silver nitrate ($AgNO_3$, 99.99%), titanium-(IV)(triethanolaminato)isopropoxide ($C_9H_{19}NO_4Ti$, 80 wt % in isopropanol), nitric acid (HNO_3), and *N*,*N*-dimethylformamide (DMF, >99.8%) were purchased from Sigma-Aldrich and used as obtained. Hydrogen peroxide (H_2O_2), liquid ammonia (liq. NH_3), and NaCl were purchased from Luba India, and isopropyl alcohol was purchased from Merck, all of which were used as provided.

2.2. Synthesis of Ag@TiO_2 Nanoparticles (NPs). A colloidal solution of Ag@TiO_2 NPs was synthesized by a modified procedure reported in previous literature.[17] In a typical synthesis, 10 mL of DMF was placed in a 100 mL double-necked round-bottom flask and heated at 150 °C under reflux conditions with magnetic stirring. Then, a freshly prepared 2 mL of 15 mM solution of $AgNO_3$ in isopropanol was added dropwise into the flask. The solution was left under reflux conditions until a yellowish color appeared. At this stage of the reaction, 2 mL of 7.5 mM titanium(IV)-(triethanolaminato)isopropoxide (TTEAIP) solution in isopropanol was added dropwise. The reaction was stopped when the reaction mixture changed from yellowish to bluish-black. The final product was cooled to room temperature and subjected to further purification.

2.3. Purification of Colloidal Ag@TiO_2 NPs. The as-synthesized colloidal NPs contained unreacted DMF and TTEAIP, which were removed by diluting the colloidal solution with ethanol, followed by centrifugation at 8000 rpm. The precipitate was collected and redispersed in ethanol by sonication. This process was repeated 8 times to completely remove the excess reagents. The NPs suspended in ethanol were air-dried and placed in a vacuum oven for 6 h. The dried particles were stored in a glass vial for further characterization.

2.4. Deposition of Colloidal Ag@TiO_2 NPs on Quartz and Glass Substrates. 5.0 mg of dried NPs was redispersed in 5 mL of isopropanol to make a solution concentration of 1 mg/mL by vortexing and sonication, respectively. Then, using a glass syringe, colloidal NPs were deposited either on glass or quartz slides by the drop-casting method. The films of the deposited NPs on the substrates were dried by airflow at room temperature.

2.5. Etching of Ag@TiO_2 NPs. Etching of Ag@TiO_2 NPs was carried out using 0.4 M HNO_3 solution (either in isopropyl alcohol or water). Initially, 5.0 mg of dried Ag@TiO_2 NPs were added into a test tube containing 5.0 mL of 0.4 M HNO_3 solution with sonication. A solution containing Ag@TiO_2 NPs dispersed either in water or isopropanol was used as the reference sample (termed the before-etching sample). During the reaction, a visual change of the reaction mixture was noticed, and UV−vis extinction spectra were recorded before etching and during the etching at different time intervals. The desired etching time was selected by observing the extinction spectrum of the sample. The Ag@TiO_2 NPs were etched at the optimized etching time, washed with a water/ethanol mixture (1:1) six times using a centrifuge machine, followed by vacuum drying, and stored in a glass vial.

2.6. UV−Visible Spectral Analysis. UV−visible spectra of both colloidal and solid-supported NPs were recorded by using a Shimadzu 1800 spectrophotometer, and the data were further processed by UV Probe software.

2.7. X-Ray Diffraction Analysis (XRD). XRD data were collected by a Rigaku SmartLab Powder Diffractometer available at SUST. Experimental X-ray generator properties: 45 kV, 200 mA; target metal: Cu; D/Ultra-250 detector, and the scanning speed is 20.00°/min. The powder sample was mounted for XRD analysis to determine the reflecting plane of the nanoparticles.

2.8. Zeta Potential Measurement. The zeta potential of colloidal Ag@TiO_2 NPs was measured using a Nanoparticle Size Analyzer (nanoParticlesSZ-100-S2, HORIBA Scientific Ltd., Japan) by the dynamic light scattering (DLS) method available at BCSIR, Dhaka. The temperature was 22.5 °C, and the dispersion medium (solvent: isopropanol) had viscosity, conductivity, and applied electrode voltage values of 0.893 mPa·s, 0.215 mS/cm, and 3.4 V, respectively.

2.9. Scanning Electron Microscopy (SEM) Coupled with Energy Dispersive Spectroscopy (EDS). The morphology and elemental analysis were carried out using a ZEISS LEO 1430 VP SEM machine, available at the Bangladesh University of Engineering and Technology (BUET), Dhaka.

2.10. Transmission Electron Microscopy (TEM) Analysis. The core−shell structure of Ag@TiO_2 NPs and the dimensions of the core (Ag) and shell (TiO_2) were determined by TEM images (model: JEM-2100 Plus Electron Microscope, Japan) available at the BCSIR in Dhaka.

2.11. Adsorption and Photocatalytic Studies. The adsorption behavior of methylene blue (MB) onto three samples: (i) TiO_2 P25, (ii) Ag@TiO_2 (unetched), and (iii) Ag@TiO_2 (etched) was studied by Langmuir and Freundlich isothermal models. First, a series of MB solutions (aqueous) having different concentrations (5 mg L^{-1}, 10 mg L^{-1}, 15 mg L^{-1}, and 20 mg L^{-1}) were prepared, and an aliquot (2.0 mL) of these solutions was extracted to measure the absorbance (at 664 nm) by a UV−vis absorption spectrophotometer. The measured absorbance data were used to draw a calibration curve using the Beer−Lambert law. In the next step, 5.0 mg of each sample was added to 100 mL of each solution. A pH of 8.5 was maintained in all solutions by adding a small amount of HCl/NaOH. The glass beakers containing the resultant solutions were left under magnetic stirring in a dark place for

https://doi.org/10.1021/acsomega.4c10276
ACS Omega 2025, 10, 14940−14948

Scheme 1. Visual Color Change (Top) of Ag@TiO_2 NPs at Different Etching Time Intervals[a]

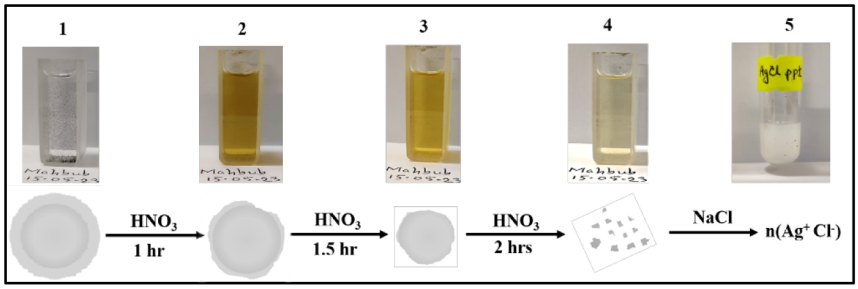

[a]Schematic representation of morphological changes in Ag@TiO_2 NPs during etching (bottom). [b]Copyright: this scheme was drawn by Mahabubur Rahman.

25 min, the time required to reach adsorption−desorption equilibrium. Once the equilibrium was established, an aliquot (2.0 mL) of each MB solution was extracted to measure the absorbance, and the corresponding equilibrium concentrations (C_e) were estimated from the calibration curve. The value of C_e was used to calculate Q_e, the amount of adsorbate adsorbed per gram of adsorbent (mg/g). K_L is the Langmuir constant (L/mg), Q_o is the maximum amount of adsorbate adsorbed per gram of adsorbent (mg/g), and b is the adsorption capacity of the adsorbent (L/mg). In addition, the $1/n$ value indicates the surface heterogeneity of the adsorbent. The obtained data were fitted to the Langmuir and Freundlich isotherm models by the following eqs 1 and 2, respectively.[18,19]

$$\frac{C_e}{Q_e} = \frac{C_e}{Q_o} + \frac{1}{K_L Q_o} \quad (1)$$

$$\ln Q_e = \ln b + \frac{1}{n}\ln C_e \quad (2)$$

To study the photocatalytic activities of the three samples, photocatalytic degradation of MB by each of the samples was investigated. Briefly, 100 mL of MB solution (1.0 mg/L), each containing 5 mg of each sample (TiO_2 P25, unetched Ag@TiO_2 NPs, and etched Ag@TiO_2 NPs), were exposed after the adsorption−desorption equilibrium was reached to either sunlight (intensity of 392 W/m^2 measured by a Digital Lux Meter, Model: LX1330B) or UV black light (4 W). An aliquot of 2.0 mL was taken at different irradiation times, centrifuged to separate the particles, and the UV−vis spectra were collected. To obtain kinetic parameters, estimated concentrations (C_t) at different degradation times (t) were fitted using the Langmuir−Hinshelwood model according to eq 3.[20]

$$\ln\left(\frac{C_o}{C_t}\right) = k_{app} t \quad (3)$$

Where, C_o is the initial concentration, and C_t indicates the concentration at time t. The apparent rate constant value, k_{app} (min^{-1}), is estimated from the gradient of the $\ln(C_o/C_t)$ vs t graph.

2.12. Raman Scattering Measurements. Powder samples of TiO_2 P25, etched Ag@TiO_2, and unetched Ag@TiO_2 were suspended in 1 mL of isopropyl alcohol containing 10 μM of the Raman probe molecule, 4-aminothiophenol. The suspensions were sonicated for 15 min to ensure proper dispersion and then left to settle overnight. Clean glass coverslips were prepared by sonication in isopropanol for 15 min, followed by drying with nitrogen gas. A 100 μL aliquot of each suspension was carefully drop-cast onto the coverslips, ensuring even distribution across the surface. After drying, the coverslips were rinsed with water to remove any unbound molecules and dried again with nitrogen gas. Raman and surface-enhanced Raman spectroscopy (SERS) measurements were performed using an Olympus IX73 inverted optical microscope. A 20× objective was used to focus circularly polarized 12.5 mW of 532 nm laser light onto the nanoparticle samples supported by the glass substrate. Raman scattered light was collected in a backscattering geometry and filtered using a dichroic mirror and a long-pass filter. Raman spectra were recorded using a Teledyne Princeton Instruments IsoPlane 320 imaging spectrograph with a 600 g/mm grating (750 nm blaze) coupled with an EM-CCD camera (ProEM-HS: 1024B). The spectra were obtained by averaging the collected light over a 200 s acquisition time period.

3. RESULTS AND DISCUSSION

3.1. Characterization of Ag@TiO_2 NPs. Metals dissolve in acidic solutions because of oxidation. Coating metal nanoparticles with inert materials such as TiO_2 delays oxidation depending on the pH of the medium.[21] This simple reaction was employed to infer the core−shell structure formation of Ag@TiO_2 NPs.

Initially, 0.4 M HNO_3 was added to a colloidal solution of Ag@TiO_2 NPs in isopropanol, and the visual color change (Scheme 1) as well as LSPR absorption spectra were recorded at different etching times (Figure 1). As can be seen in Scheme 1 (top), the black Ag@TiO_2 NPs were suspended in isopropanol, which slowly turned into dark yellow to pale yellow and finally into a transparent solution. The addition of NaCl solution turned the transparent solution into a white suspension, indicating the formation of AgCl from Ag^+ ions.

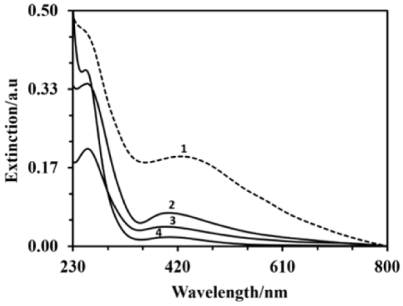

Figure 1. UV−vis extinction spectra of Ag@TiO_2 NPs during the etching process indicate a blue shift (size reduction) of LSPR.

https://doi.org/10.1021/acsomega.4c10276
ACS Omega 2025, 10, 14940−14948

The corresponding absorption spectrum of Ag@TiO_2 NPs showed the presence of the LSPR band centered at 436 nm (Figure 1). Blue shifting of the LSPR peak and a decrease of band intensity revealed that the TiO_2 shell was etched by acid, which finally oxidized Ag^0 into Ag^+ ions. The slow etching of particles by acid was because of the high viscosity of isopropanol, which resulted in low diffusion of reactants. The gradual color change and LSPR peak shifting revealed that initially, the shell protected the core Ag NPs from corrosion, and once the core became uncapped, it started dissolving in the acid solution.

3.2. X-Ray Diffraction (XRD) Analysis. The crystalline structure of the as-prepared Ag@TiO_2 NPs was determined by powder XRD. Figure 2 illustrates the XRD patterns of the Ag@

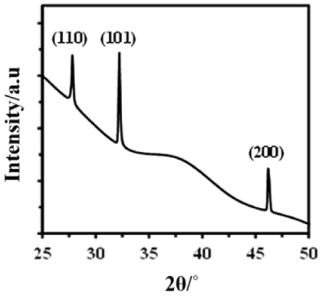

Figure 2. XRD pattern of the as-synthesized Ag@TiO_2 NPs.

TiO_2 NPs. The diffraction peak of core-Ag in Ag@TiO_2 NPs appeared at 46.36°, which corresponded to the (200) lattice planes of a face-centered cubic (fcc) Ag crystal. In the case of TiO_2 (shell), the diffraction pattern exhibited characteristic peaks of both anatase and rutile phases. The peaks at 27.85° and 32.36° corresponded to the (110) and (101) lattice planes of the rutile and anatase phases of TiO_2, respectively.[22] The details of the XRD data are given in the Supporting Document S6. However, some peaks corresponding to the (111), (211), (200), and (303) planes of TiO_2 are absent in the XRD diffractogram, which indicates the formation of defective/amorphous TiO_2.[22]

3.3. SEM-EDS and TEM Analysis of the Ag@TiO_2 NPs. The core−shell structure was further confirmed by SEM-EDS (Figure 3) and TEM (Figure 4). The EDS analysis showed

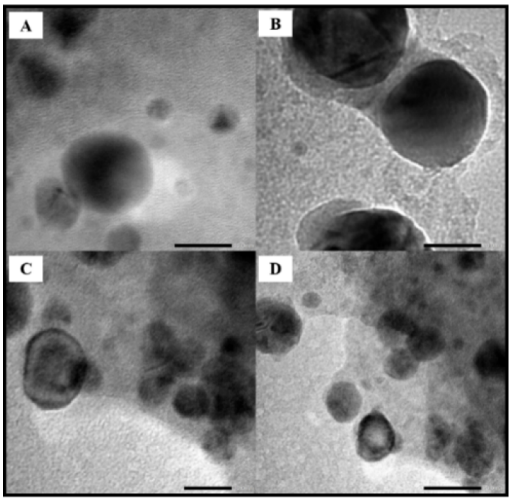

Figure 4. TEM images of Ag@TiO_2 NPs (A, B) before etching and (C, D) after etching.

that the chemical composition of the particles consisted of Ag, Ti, and oxygen. The SEM image indicated the formation of larger aggregates, which was because of the insufficient stability of colloidal particles, as revealed by the lower zeta potential.

3.4. Zeta Potential of the Ag@TiO_2 NPs. The surface charge of the nanoparticles is an essential parameter to understand the stability of particles in a dispersant. The application of the NPs in various fields is largely dependent on the surface charge, which can be determined from the value of zeta potential. Particles with a zeta potential more positive than +30 mV or more negative than −30 mV indicate higher stability in solution.[23] The experimental zeta potential for Ag@TiO_2 NPs was found to be −18.4 mV (Figure 5) in isopropyl alcohol, indicating that the particles were moderately stable in that solvent.

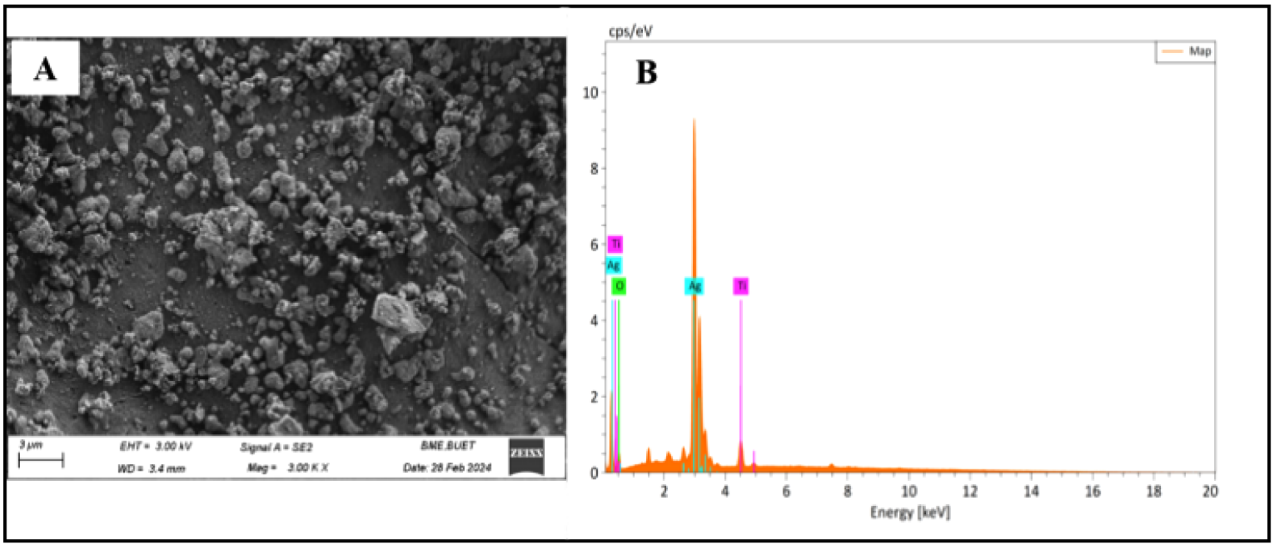

Figure 3. SEM image (A) of the aggregated Ag@TiO_2 NPs, and EDS spectra (B) showing the presence of Ag, Ti, and O.

https://doi.org/10.1021/acsomega.4c10276
ACS Omega 2025, 10, 14940−14948

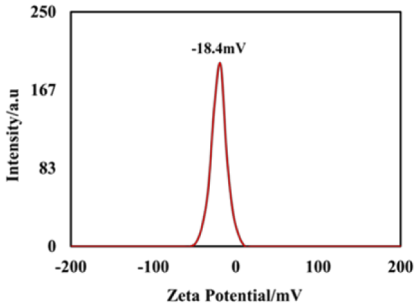

Figure 5. Zeta potential distribution graph depicting a negative zeta potential (−18.4 mV) for Ag@TiO_2 NPs.

3.5. Correlating Optical Properties of Ag@TiO_2 NPs with Their Shell Thicknesses. Silver nanoparticles can support localized surface plasmon resonance (LSPR) modes in a wide range of spectral wavelengths (300−1200 nm), depending on their size, shape, and refractive index of the surrounding media.[1,24,25] Herein, the position of the LSPR absorption of the studied Ag@TiO_2 NPs, with specific size and shape, depends on the shell (TiO_2) thickness (the dielectric material in contact with the plasmonic core, Ag). Acid etching reduces the shell material of Ag@TiO_2 NPs, which alters the LSPR absorption of light. To study the shell-thickness-dependent LSPR behavior of colloidal Ag@TiO_2 NPs, dried Ag@TiO_2 NPs were dispersed in 0.4 M HNO_3 solution (aq) under sonication and vortexing to make a colloidal solution. LSPR absorption spectra of colloidal particles were recorded during acid etching at different time intervals. For the reference LSPR spectrum, a colloidal solution containing 1 mg/mL of Ag@TiO_2 in distilled water was used. The change of LSPR absorption spectra, before and after etching, is shown in Figure 6. It is evident that the reference spectrum consisted of two

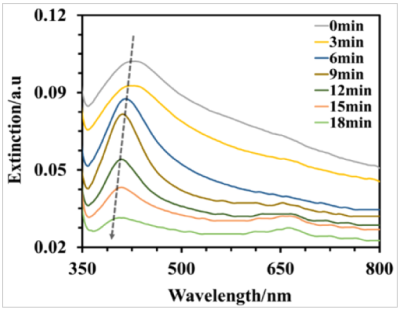

Figure 6. LSPR spectra of Ag@TiO_2 NPs in water during etching in 0.4 M HNO_3 solution.

spectral bands: one centered at 430 nm, which originated from the LSPR absorption of Ag NPs with a diameter of ∼10 nm, and the second features a shoulder at 655 nm, which might have originated from the scattering of light by TiO_2.[26,27] The intensity and LSPR peak position of the band at 430 nm decreased and blue-shifted, respectively. A blue shift in the LSPR absorption peak indicates the size reduction of Ag@TiO_2 NPs because of the erosion of TiO_2 from the shell. During the etching process, a state was reached where the core Ag particles were completely exposed, and the absorption band became sharper, eventually leading to the complete dissolution of Ag^0 to Ag^+, which lowered the LSPR absorption intensity. However, the intensity of the band at 655 nm was found to increase, which was because of an increase in TiO_2 density in the solution with etching time.

Often, certain applications require the deposition of nanostructures on solid supports as a technical requirement as well as for the discovery of new plasmonic properties.[28,29] In colloidal solutions, the particles exist in a symmetrical dielectric environment, but when they are on solid supports, the particles remain at fixed positions and in an asymmetric dielectric environment. Therefore, the generation of new optical properties, evolved from interparticle plasmon coupling and substrate-induced plasmon hybridization, is expected.[30,31] Since the Ag core is already encapsulated with TiO_2 in an unetched sample, its plasmonic absorption depends on shell thickness. On the other hand, the etched sample is partially encapsulated, which enables it to interact with the substrate. To investigate the LSPR properties of solid-supported Ag@TiO_2 NPs, both unetched and etched NPs were deposited on quartz slides, and their UV−vis spectra were collected.

To separate LSPR absorption bands from any absorption/scattering signals of the TiO_2 shell, a film of TiO_2 P25 was deposited on a quartz slide along with Ag samples. As can be seen from Figure 7, the TiO_2 P25 film showed two distinct

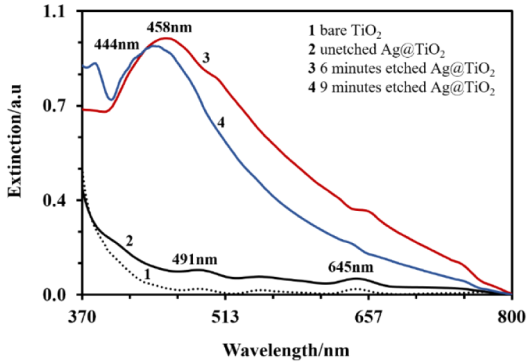

Figure 7. SPR spectra of the (1) bare TiO_2 NPs, (2) unetched Ag@TiO_2 NPs, (3) 6 min-etched Ag@TiO_2 NPs, and (4) 9 min-etched Ag@TiO_2 NPs on the quartz support.

bands in the absorption spectrum: one at 491 nm (interband transition) and the other at 645 nm (scattering). The extinction spectrum of the film consisting of Ag@TiO_2 NP film exhibited similar spectral features to those of the TiO_2 P25 film. Interesting spectral features appeared with the film consisting of 6 min-etched Ag@TiO_2 NPs. The spectrum consisted of a band centered at 458 nm corresponding to the LSPR absorption of core silver NPs and a less intense band at 645 nm, which corresponds to the scattering band of the TiO_2 shell. However, Ag@TiO_2 NPs that were subjected to 9 min of etching exhibited a blue-shifted Ag LSPR band, and the scattering peak almost disappeared. The TEM image (Figure 5) of unetched Ag@TiO_2 showed the formation of spherical nanoparticles with ∼20 nm diameters encapsulated with an ∼7 nm TiO_2 shell. After 6 min of etching, the NPs reduced to smaller and irregularly shaped particles. Most of the particles were partially encapsulated, which indicated that the etching process was not homogeneous. Because of drop casting, the particles formed a multilayered film, and the unetched Ag@TiO_2 with a thicker shell exhibited spectral features of pristine TiO_2. The incident light could not excite the core silver plasmons. The film with 6 min-etched particles having a partially exposed Ag core or fully exposed Ag nanoparticles

https://doi.org/10.1021/acsomega.4c10276
ACS Omega 2025, 10, 14940−14948

exhibited the Ag plasmonic absorption as well as the optical response from the partially covered TiO_2 shell. After longer etching times, when the TiO_2 shell was completely removed, the spectral feature consisted of the core Ag plasmonic response, which eventually disappeared because of the disintegration of Ag nanoparticles into Ag^+ ions. Therefore, the Ag@TiO_2 NPs showing the spectral features of both the Ag core LSPR band and TiO_2 scattering band would be the core−shell nanostructures with optimized thickness.

3.6. SERS Response of Different Ag@TiO_2 NP Samples. Due to the electromagnetic field gradient at the surface of plasmonically excited Ag, the enhancement of Raman scattering is expected to depend on the shell thickness of Ag@TiO_2 samples, which serves as a spacer between a Raman probe and the Ag surface.

The Raman spectra of 4-aminothiophenol were measured on etched and unetched Ag@TiO_2 samples supported on glass substrates to determine whether a decreased TiO_2 shell thickness supports SERS. To separate the Raman signal of the TiO_2 shell from that of 4-aminothiophenol probe molecules, the Raman spectra of TiO_2 P25 particles were collected. Raman and SERS signals of the three samples are shown in Figure 8. The Raman spectra of TiO_2 P25 samples

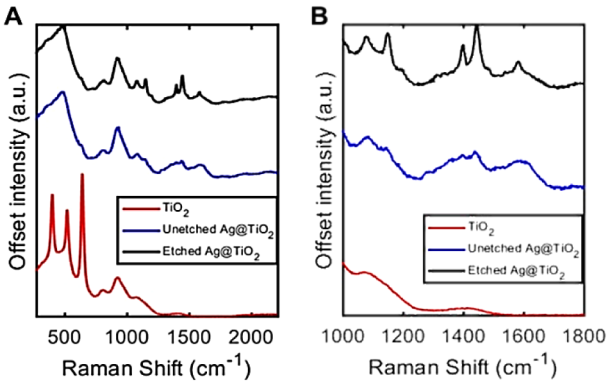

Figure 8. (A) Raman and SERS spectra of TiO_2 (red curve) and 4-aminothiophenol adsorbed onto etched (black curve) and unetched (blue curve) Ag@TiO_2. (B) Zoomed-in spectral window highlighting the vibrational modes of adsorbed 4-aminothiophenol.

consisted of distinct Raman peaks corresponding to the Ti−O stretching (642 cm^{-1}) and O−Ti−O bending modes (403 and 518 cm^{-1}) as shown in Table 3.[32] These fingerprint Raman peaks of TiO_2 are less intense in Ag@TiO_2 samples (both etched and unetched), which might be because of its amorphous nature. XRD and TEM results are consistent with the formation of an amorphous TiO_2 shell on the core Ag during the synthesis of Ag@TiO_2 NPs. Vibrational modes from 4-aminothiophenol were observed in both Ag@TiO_2 core−shell samples (Figure 8 and Table 1).

The Raman signal of 4-aminothiophenol from etched Ag@TiO_2 was greater than that of unetched Ag@TiO_2. Assuming the same coverage of 4-aminothiophenol on the etched and unetched Ag@TiO_2 samples, this result indicates that Raman scattering is enhanced by etched Ag@TiO_2. In the case of unetched Ag@TiO_2, 4-aminothiophenol molecules adsorb onto the shell surface, ∼7 nm away from the Ag core, and therefore experience a lower EM field, yielding lower intensities of Raman scattered light. In the case of the etched sample, Ag@TiO_2 with a thinner shell and/or a partially

Table 1. Tabulated Vibrational Modes Measured by Raman/SERS[a]

Measured Raman modes (cm^{-1})		
TiO_2	Unetched Ag@TiO_2	Etched Ag@TiO_2
403	491	491
518	810	817
642	924	916
802	1085	1073
928	1139	1155
1089	1279	1191
1414	-	1311
	1405	1395
	1438	1442
	1591	1574

[a]TiO_2 modes are marked in red, and 4-aminothiophenol modes are in bold font.

exposed Ag core enables 4-aminothiophenol to adsorb closer to or directly on Ag, resulting in enhanced Raman scattering from the greater EM field. In addition, direct adsorption of 4-aminothiophenol onto Ag may result in a chemical enhancement of Raman scattering.[33] The large EM field and potential chemical enhancement both result in larger Raman signals from etched Ag@TiO_2.

3.7. Photocatalytic Activities of Ag@TiO_2 Samples. Adsorption is a prerequisite for heterogeneous catalysis. Therefore, the adsorption of methylene blue (MB) in aqueous solution onto Ag@TiO_2 samples and TiO_2 P25 was studied before investigating their catalytic activities (Figure 9A,B). The spectral data and different parameters associated with the adsorption study are given in Supporting Information S1, S2, and S3 and Table 2, respectively. The results revealed that MB adsorption on TiO_2 P25 followed the Langmuir isotherm model, indicating the formation of a monolayer, which is consistent with previous reports.[34] On the other hand, the adsorption behavior of both Ag@TiO_2 samples (unetched and etched) followed the Freundlich isotherm model, which implied the formation of a multilayer. The dissimilarity in the adsorption behavior among the three samples is related to their morphologies. During the formation of heterostructured Ag@TiO_2 particles, the radial growth of the TiO_2 (shell) around the core (Ag) was not uniform, which created heterogeneities on the surface. Further surface heterogeneity was generated by the chemical etching of Ag@TiO_2 NPs. TEM images revealed that the surfaces of both Ag@TiO_2 NPs were rough; the presence of apexes and troughs might have stimulated multilayer formation. However, single-component TiO_2 P25 (d = ∼20 nm) particles had a smoother surface, which led to the formation of the monolayer.

Further studies on the photocatalytic activity of the samples were conducted to unveil the involvement of the plasmonic effect. For this purpose, photodegradation (under solar illumination) of the MB dye by three samples was studied (spectral data are given in Supporting Information S4). The degradation kinetics were modeled with the Langmuir−Hinshelwood equation (eq 1) as shown in Figure 9C, and the kinetic parameters are listed in Table 3. It is evident that etched Ag@TiO_2 exhibited a 5-fold faster rate constant than that of TiO_2 P25. The faster rate constant of etched Ag@TiO_2 NPs can be explained by the thinner shell (∼2 nm), which allowed incident light to excite the LSP of core silver and subsequently transfer hot electrons to the conduction band of

https://doi.org/10.1021/acsomega.4c10276
ACS Omega 2025, 10, 14940−14948

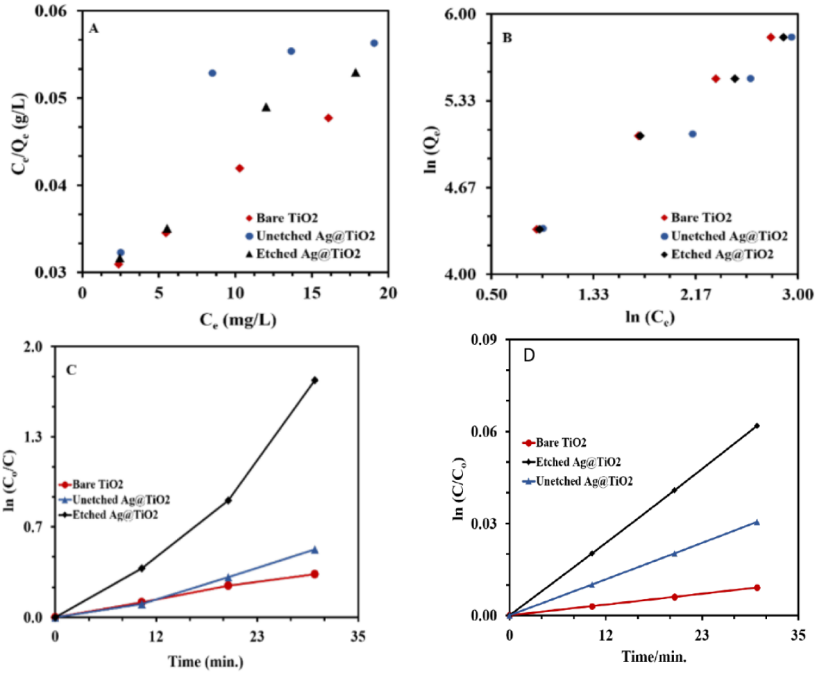

Figure 9. Langmuir and Freundlich adsorption isotherms (A, B) of three samples. Langmuir−Hinshelwood degradation kinetics of three samples under (C) sunlight and (D) UV light.

Table 2. Parameters of Langmuir and Freundlich Adsorption Isotherms for the Adsorption of MB on Samples under Dark Conditions

Isotherm models	Langmuir		Freundlich		
Parameters	R^2	K_L (L/mg)	R^2	1/n	b (L/mg)
bare TiO_2 P25 (dark)	0.9916	0.04626	0.9967	0.7698	40.68
unetched Ag@TiO_2 NPs (dark)	0.7417	0.04106	0.9863	0.7123	38.68
etched Ag@TiO_2 NPs (dark)	0.9576	0.05319	0.9918	0.7231	42.17

Table 3. Langmuir−Hinshelwood Kinetic Parameters for Photocatalytic Degradation (Solar Intensity: 392 Wm^{-2}) of MB onto Three Samples

Sample	K_{app} (min^{-1})
bare TiO_2	0.0108
unetched Ag@TiO_2 NPs	0.0170
etched Ag@TiO_2 NPs	0.0575

TiO_2. The increased charge carriers in the TiO_2 semiconductor enhanced the degradation rate. The detailed mechanism of the reaction pathways is described elsewhere.[35] Recently, the plasmonic-heating effect, because of LSPR excitation by light, has been reported to play a key role in the increased reaction (degradation) rate.[36] However, the reaction rate exhibited by the unetched Ag@TiO_2 NPs resembled that of TiO_2 P25.

This is because the thicker shell (∼7 nm) hindered the penetration of incident light through it, due to which the LSP of the core silver was not excited, and hence the photocatalytic activity of unetched Ag@TiO_2 NPs exhibited an identical value to that of TiO_2 P25.

On the contrary, the photocatalytic activities of the three samples under UV light irradiation (intensity: 0.351 W/m^2) exhibited a significantly lower degradation rate compared to those under sunlight irradiation, as shown in Figure 9D. Spectral data are given in Supporting Information S5. However, the increasing trend of photocatalytic activities for the three samples followed the same order as those under sunlight irradiation (Table 4). The observed lower degradation rate might be because of the lower intensity of incident UV light (0.351 Wm^{-2}) as well as the excitation of only the high energy (365 nm) surface plasmon of core-Ag nanostructures. The increasing trend of the photodegradation rate of MB can be explained by the involvement of plasmonic energy with Ag@TiO_2 samples.

Table 4. Langmuir−Hinshelwood Kinetic Parameters for Photocatalytic Degradation (UV Intensity: 0.351 Wm^{-2}) of MB onto Three Samples

Sample	K_{app} (min^{-1})
bare TiO_2	0.0003
unetched Ag@TiO_2 NPs	0.0011
etched Ag@TiO_2 NPs	0.0021

4. CONCLUSIONS

Herein, we described a simple acid etching method to manipulate the shell thickness of Ag@TiO_2 core−shell nanoparticles (d = ∼20 nm) to achieve optimized plasmonic properties, which were exploited to fabricate novel plasmonic photocatalysts and SERS substrates. The novelty of this method is that the UV−vis extinction spectrum can be used to prepare Ag@TiO_2 NPs with the desired thickness. The concurrent existence of the LSPR band of the core silver (d = ∼10 nm) and the scattering peak of the shell (∼2 nm) TiO_2 in the extinction spectrum was considered as the intended morphology of the NPs. Although the etching process could not produce a homogeneous shell thickness in Ag@TiO_2 NPs,

https://doi.org/10.1021/acsomega.4c10276
ACS Omega 2025, 10, 14940−14948

nevertheless, the NPs exhibited enhanced photocatalytic and SERS activities. This method could be extended to other core−shell NPs consisting of core metal@semiconductor shell nanostructures, which find applications in plasmonic solar cells, nanoelectronics, and plasmonic sensors.

■ ASSOCIATED CONTENT

Supporting Information

The Supporting Information is available free of charge at https://pubs.acs.org/doi/10.1021/acsomega.4c10276.

UV−vis spectra of MB during adsorption and degradation at different concentrations and degradation times (PDF)

■ AUTHOR INFORMATION

Corresponding Author

Nur Uddin Ahamad − *Department of Chemistry, Shahjalal University of Science and Technology Sylhet, Sylhet 3114, Bangladesh;* orcid.org/0000-0002-8193-8919; Email: nur-che@sust.edu

Authors

Mahabubur Rahman − *Department of Chemistry, Shahjalal University of Science and Technology Sylhet, Sylhet 3114, Bangladesh;* orcid.org/0009-0008-2692-7548

Md Al-Amin − *College of Arts and Science, Department of Chemistry, University of Louisville, Louisville, Kentucky 40208, United States*

Amandeep Kaur − *College of Arts and Science, Department of Chemistry, University of Louisville, Louisville, Kentucky 40208, United States*

Shirin Akter Jahan − *Bangladesh Council for Scientific and Industrial Research, Bangladesh (BCSIR), Institute of Glass and Ceramic Research and Testing (IGCRT) Dhaka, Dhaka 1205, Bangladesh*

Andrew J. Wilson − *College of Arts and Science, Department of Chemistry, University of Louisville, Louisville, Kentucky 40208, United States;* orcid.org/0000-0003-3427-810X

Complete contact information is available at: https://pubs.acs.org/10.1021/acsomega.4c10276

Author Contributions

N.U.A. designed and supervised the research work. M.R. conducted the experiments, except for the Raman analysis, and wrote the draft copy of the manuscript. A.J.W. designed and supervised the Raman experiment and wrote the experimental and result sections. A.K. conducted the Raman experiment. M.A.A. assisted in analyzing the SEM images and participated in the overall discussion. S.J.A. recorded and analyzed the TEM images.

Funding

Financial support was provided by the SUST Research Center (Project ID: PS/2021/1/03).

Notes

The authors declare no competing financial interest.

■ ACKNOWLEDGMENTS

We would like to acknowledge Mr Omar Faruk (Department of Physics, SUST) and Prof. Abu Bin Imran (Department of Chemistry, BUET) for their experimental assistance.

■ REFERENCES

(1) Rycenga, M.; Cobley, C. M.; Zeng, J.; Li, W.; Moran, C. H.; Zhang, Q.; Qin, D.; Xia, Y. Controlling the Synthesis and Assembly of Silver Nanostructures for Plasmonic Applications. *Chem. Rev.* **2011**, *111* (6), 3669−3712.

(2) Jones, M. R.; Osberg, K. D.; Macfarlane, R. J.; Langille, M. R.; Mirkin, C. A. Templated Techniques for the Synthesis and Assembly of Plasmonic Nanostructures. *Chem. Rev.* **2011**, *111* (6), 3736−3827.

(3) Mayer, K. M.; Hafner, J. H. Localized Surface Plasmon Resonance Sensors. *Chem. Rev.* **2011**, *111* (6), 3828−3857.

(4) Tian, Y.; Tatsuma, T. Mechanisms and Applications of Plasmon-Induced Charge Separation at TiO_2 Films Loaded with Gold Nanoparticles. *J. Am. Chem. Soc.* **2005**, *127* (20), 7632−7637.

(5) Atwater, H. A.; Polman, A. Plasmonics for Improved Photovoltaic Devices. *Nat. Mater.* **2010**, *9* (3), 205−213.

(6) Li, J.; Cushing, S. K.; Bright, J.; Meng, F.; Senty, T. R.; Zheng, P.; Bristow, A. D.; Wu, N. Ag@Cu_2O Core-Shell Nanoparticles as Visible-Light Plasmonic Photocatalysts. *ACS Catal.* **2013**, *3* (1), 47−51.

(7) Quiñones Vélez, G.; París Santiago, A.; Soto Nieves, D.; Figueroa Guzmán, A.; Peterson-Peguero, E.; López-Mejías, V. Functionalization of Titanium Dioxide by *In Situ* Surface Crystallization of Bisphosphonate-Based Coordination Complexes. *Inorg. Chem.* **2023**, *62* (1), 201−212.

(8) Gonzalez-Calderon, J. A.; Fierro-Gonzalez, J. C.; Peña-Juarez, M. G.; Perez, E.; Almendarez-Camarillo, A. Influence of the Chemical Functionalization of Titanium Oxide Nanotubes on the Non-Isothermal Crystallization of Polypropylene Nanocomposites. *J. Mater. Sci.* **2022**, *57* (10), 5855−5872.

(9) Schmitt, L.; Ludwig, M.; Gaub, H. E.; Tampé, R. A Metal-Chelating Microscopy Tip as a New Toolbox for Single-Molecule Experiments by Atomic Force Microscopy. *Biophys. J.* **2000**, *78* (6), 3275−3285.

(10) Kneipp, J.; Kneipp, H.; Wittig, B.; Kneipp, K. Following the Dynamics of pH in Endosomes of Live Cells with SERS Nanosensors. *J. Phys. Chem. C* **2010**, *114* (16), 7421−7426.

(11) Shao, Y.; Xu, S.; Zheng, X.; Wang, Y.; Xu, W. Optical Fiber LSPR Biosensor Prepared by Gold Nanoparticle Assembly on Polyelectrolyte Multilayer. *Sensors* **2010**, *10* (4), 3585−3596.

(12) Clavero, C. Plasmon-Induced Hot-Electron Generation at Nanoparticle/Metal-Oxide Interfaces for Photovoltaic and Photocatalytic Devices. *Nat. Photonics* **2014**, *8* (2), 95−103.

(13) Michaelson, H. B. The Work Function of the Elements and Its Periodicity. *J. Appl. Phys.* **1977**, *48* (11), 4729−4733.

(14) Linic, S.; Christopher, P.; Ingram, D. B. Plasmonic-Metal Nanostructures for Efficient Conversion of Solar to Chemical Energy. *Nat. Mater.* **2011**, *10* (12), 911−921.

(15) Schneider, G.; Decher, G. Functional Core/Shell Nanoparticles via Layer-by-Layer Assembly. Investigation of the Experimental Parameters for Controlling Particle Aggregation and for Enhancing Dispersion Stability. *Langmuir* **2008**, *24* (5), 1778−1789.

(16) Yu, Z.; Tetard, L.; Zhai, L.; Thomas, J. Supercapacitor Electrode Materials: Nanostructures from 0 to 3 Dimensions. *Energy Environ. Sci.* **2015**, *8* (3), 702−730.

(17) Hirakawa, T.; Kamat, P. V. Photoinduced Electron Storage and Surface Plasmon Modulation in Ag@TiO_2 Clusters. *Langmuir* **2004**, *20* (14), 5645−5647.

(18) Kalam, S.; Abu-Khamsin, S. A.; Kamal, M. S.; Patil, S. Surfactant Adsorption Isotherms: A Review. *ACS Omega* **2021**, *6* (48), 32342−32348.

(19) Liu, L.; Gao, Z. Y.; Su, X. P.; Chen, X.; Jiang, L.; Yao, J. M. Adsorption Removal of Dyes from Single and Binary Solutions Using a Cellulose-Based Bioadsorbent. *ACS Sustainable Chem. Eng.* **2015**, *3* (3), 432−442.

(20) Asenjo, N. G.; Santamaría, R.; Blanco, C.; Granda, M.; Álvarez, P.; Menéndez, R. Correct Use of the Langmuir−Hinshelwood Equation for Proving the Absence of a Synergy Effect in the Photocatalytic Degradation of Phenol on a Suspended Mixture of Titania and Activated Carbon. *Carbon* **2013**, *55*, 62−69.

(21) Zhang, C.; Sun, X.; Li, J.; Liu, Y.-N. Synthesis of Ag Nanoclusters by a pH-Dependent Etching Method in Aqueous Solution. *Nanoscale* **2013**, *5* (14), 6261.
(22) Sayed, M.; Shi, Z.; Gholami, F.; Fatehi, P.; Soliman, A. I. A. Ag@TiO_2 Nanocomposite as an Efficient Catalyst for Knoevenagel Condensation. *ACS Omega* **2022**, *7* (36), 32393−32400.
(23) Pinto, I.; Buss, A. ζ Potential as a Measure of Asphalt Emulsion Stability. *Energy Fuels* **2020**, *34* (2), 2143−2151.
(24) Liu, D.-Y.; Ding, S.-Y.; Lin, H.-X.; Liu, B.-J.; Ye, Z.-Z.; Fan, F.-R.; Ren, B.; Tian, Z.-Q. Distinctive Enhanced and Tunable Plasmon Resonant Absorption from Controllable Au@Cu_2O Nanoparticles: Experimental and Theoretical Modeling. *J. Phys. Chem. C* **2012**, *116* (7), 4477−4483.
(25) Zhang, L.; Wang, H. Cuprous Oxide Nanoshells with Geometrically Tunable Optical Properties. *ACS Nano* **2011**, *5* (4), 3257−3267.
(26) Mogensen, K. B.; Kneipp, K. Size-Dependent Shifts of Plasmon Resonance in Silver Nanoparticle Films Using Controlled Dissolution: Monitoring the Onset of Surface Screening Effects. *J. Phys. Chem. C* **2014**, *118* (48), 28075−28083.
(27) Mahmoud, M. A.; Qian, W.; El-Sayed, M. A. Following Charge Separation on the Nanoscale in Cu_2O−Au Nanoframe Hollow Nanoparticles. *Nano Lett.* **2011**, *11* (8), 3285−3289.
(28) Zhang, S.; Bao, K.; Halas, N. J.; Xu, H.; Nordlander, P. Substrate-Induced Fano Resonances of a Plasmonic Nanocube: A Route to Increased-Sensitivity Localized Surface Plasmon Resonance Sensors Revealed. *Nano Lett.* **2011**, *11* (4), 1657−1663.
(29) Ahamad, N.; Bottomley, A.; Ianoul, A. Optimizing Refractive Index Sensitivity of Supported Silver Nanocube Monolayers. *J. Phys. Chem. C* **2012**, *116* (1), 185−192.
(30) Kim, S.; Jin, J.; Kim, Y.-J.; Park, I.-Y.; Kim, Y.; Kim, S.-W. High-Harmonic Generation by Resonant Plasmon Field Enhancement. *Nature* **2008**, *453* (7196), 757−760.
(31) Lassiter, J. B.; Aizpurua, J.; Hernandez, L. I.; Brandl, D. W.; Romero, I.; Lal, S.; Hafner, J. H.; Nordlander, P.; Halas, N. J. Close Encounters between Two Nanoshells. *Nano Lett.* **2008**, *8* (4), 1212−1218.
(32) Taudul, B.; Tielens, F.; Calatayud, M. On the Origin of Raman Activity in Anatase TiO_2 (Nano) Materials: An Ab Initio Investigation of Surface and Size Effects. *Nanomaterials* **2023**, *13* (12), 1856.
(33) Hu, X.; Wang, T.; Wang, L.; Dong, S. Surface-Enhanced Raman Scattering of 4-Aminothiophenol Self-Assembled Monolayers in Sandwich Structure with Nanoparticle Shape Dependence: Off-Surface Plasmon Resonance Condition. *J. Phys. Chem. C* **2007**, *111* (19), 6962−6969.
(34) Mousavi, S. H.; Shokoofehpoor, F.; Mohammadi, A. Synthesis and Characterization of γ-CD-Modified TiO_2 Nanoparticles and Its Adsorption Performance for Different Types of Organic Dyes. *J. Chem. Eng. Data.* **2019**, *64* (1), 135−149.
(35) Schneider, J.; Matsuoka, M.; Takeuchi, M.; Zhang, J.; Horiuchi, Y.; Anpo, M.; Bahnemann, D. W. Understanding TiO_2 Photocatalysis: Mechanisms and Materials. *Chem. Rev.* **2014**, *114* (19), 9919−9986.
(36) Al-Amin, M.; Hemmer, J. V.; Joshi, P. B.; Fogelman, K.; Wilson, A. J. Quantification and Description of Photothermal Heating Effects in Plasmon-Assisted Electrochemistry. *Commun. Chem.* **2024**, *7* (1), 70.

https://doi.org/10.1021/acsomega.4c10276
ACS Omega 2025, 10, 14940−14948